

Nature of the metal-insulator transition in the half-filled $t - t'$ Hubbard chain

G. I. Japaridze,¹ R. M. Noack,² and D. Baeriswyl³

¹*Max-Planck-Institut für Physik komplexer Systeme, Nötnitzer Str. 38, D-01187 Dresden, Germany**

²*Fachbereich Physik, Philipps-Universität Marburg, D-35032 Marburg, Germany*

³*Département de physique, Université de Fribourg, CH-1700 Fribourg, Switzerland*

(Dated: June 28, 2006)

We study the quantum phase transition from an insulator to a metal realized at $t' = t'_c > 0.5t$ in the ground state of the half-filled Hubbard chain with both nearest-neighbor (t) and next-nearest-neighbor (t') hopping. The study is carried out using the bosonization approach and density matrix renormalization group calculations. An effective low-energy Hamiltonian that describes the insulator-metal transition is derived. We find that the gross features of the phase diagram are well-described by the standard theory of commensurate-incommensurate transitions in a wide range of parameters. We also obtain an analytical expression for the insulator-metal transition line $t'_c(U, t)$. We argue that close to the insulator-metal transition line, a crossover to a regime corresponding to an infinite-order transition takes place. We present results of density-matrix-renormalization-group calculations of spin and charge distribution in various sectors of the phase diagram. The numerical results support the picture derived from the effective theory and give evidence for the complete separation of the transitions involving spin and charge degrees of freedom.

PACS numbers: 71.27.+a, 71.30.+h

I. INTRODUCTION

During the last decades, the Mott metal-insulator transition has been the subject of great interest.^{1,2,3} In the canonical model for this transition – the single-band Hubbard model – the origin of the insulating behavior is the on-site Coulomb repulsion between electrons. For an average density of one electron per site, the transition from the metallic to the insulating phase is expected to occur when the electron-electron interaction strength U is of the order of the delocalization energy (which is a few times the hopping amplitude t). The critical value $(U/t)_c$ turns out to be quite independent of the specific band structure.⁴ It is important to recall that the Mott transition is often preceded by antiferromagnetic ordering, which usually leads to insulating behavior and thus masks the Mott phenomenon.

While the underlying mechanism driving the Mott transition is by now well understood, many questions remain open, especially about the region close to the transition point where perturbative approaches fail to provide reliable answers. The situation is more fortunate in one dimension, where non-perturbative analytical methods together with well-controlled numerical approaches allow in many cases to determine both the ground state and the low-lying excited states.^{5,6,7} However, even in one dimension, apart from the exactly solvable cases, a full treatment of the fundamental issues related to the Mott transition still constitutes a hard and long-standing problem.

In this paper, we study the $t - t'$ Hubbard chain which includes both nearest (t) and next-nearest-neighbor (t') hopping terms. We limit ourselves to an average density of one electron per site (the half-filled band case). Depending on the ratio between t' and t , the system has two or four Fermi points. Correspondingly, it shows one- or

two-band behavior and has a rich phase diagram. Therefore, it is not surprising that the model has been the subject of intensive analytical and numerical studies, including a weak-coupling renormalization group analysis,⁸ DMRG calculations for charge and spin gaps^{9,10,11,12,13}, the electric susceptibility,¹⁴ the momentum distribution function,^{15,16,17} and the conductivity¹³ as well as, very recently, a variational technique.¹⁸

Unfortunately, conflicting results have been reported for the transition region, in particular regarding the character of the transition, the number of different phases and the number of gapless modes. In this paper, we hope to settle some of the unresolved issues using a combined analytical and numerical analysis. We focus our attention on the metal-insulator transition as a function of t' for a fixed on-site repulsion U . An effective continuum theory allows us to show that in the parameter range $0.5t < t' < t'_c$ the system exhibits the characteristic behavior of a commensurate-incommensurate transition.¹⁹ Close to the transition point, additional scattering processes characteristic of two-band behavior set in.⁸ We argue that these processes induce a crossover to Kosterlitz-Thouless type critical behavior, as found in Ref. 14. Additional support for this conclusion is provided by DMRG calculations for chains of up to $L = 128$ sites and large U . The numerical analysis also allows us to study the gaps in the excitation spectrum as well as the charge and spin density distributions.

The paper is organized as follows. In Section II, general properties of the model including the strong coupling limit and the structure of the phase diagram are briefly reviewed. Section III shows that the weak-coupling bosonization approach leads to the quantum sine-Gordon field theory, the standard model for commensurate-incommensurate transitions. In Section IV, the results of the numerical analysis are presented, including the ex-

citation spectrum and density distributions. Special attention is given to the regime of large t' where the model represents a system of two coupled chains. The results are summarized in Section V.

II. THE $t - t'$ HUBBARD CHAIN

The one-dimensional $t - t'$ Hubbard model is defined by the Hamiltonian

$$\begin{aligned} \mathcal{H} = & -t \sum_{j,\sigma} \left(c_{j,\sigma}^\dagger c_{j+1,\sigma} + c_{j+1,\sigma}^\dagger c_{j,\sigma} \right) \\ & + t' \sum_{j,\sigma} \left(c_{j,\sigma}^\dagger c_{j+2,\sigma} + c_{j+2,\sigma}^\dagger c_{j,\sigma} \right) \\ & + U \sum_{j,\sigma} (n_{j,\uparrow} - 1/2)(n_{j,\downarrow} - 1/2), \end{aligned} \quad (1)$$

where $c_{j,\sigma}^\dagger$ ($c_{j,\sigma}$) are electron creation (annihilation) operators on site j and, with spin projection $\sigma = \uparrow, \downarrow$, $n_{j,\sigma} = c_{j,\sigma}^\dagger c_{j,\sigma}$, and U is the on-site Coulomb repulsion.

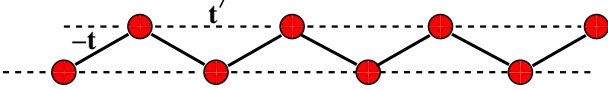


FIG. 1: The $t - t'$ Hubbard chain.

The model can be viewed either as a single chain with both nearest- and next-nearest-neighbor hopping or, as illustrated in Fig.1, as a system of two coupled chains. The former view is appropriate for $t \gg t'$, the latter for $t' \gg t$.

For $t' = 0$, we recover the ordinary Hubbard model which is exactly (Bethe Ansatz) solvable.⁵ In the case of a half-filled band, the ground state is insulating for arbitrary positive values of U ; the charge excitation spectrum is gapped while the spin excitation spectrum is gapless.^{5,6} For $U \ll t$ the charge gap Δ_c is exponentially small, $\Delta_c \approx \sqrt{U} t e^{-2\pi t/U}$, while $\Delta_c \approx U$ for $U \gg t$.⁶

For $t' \neq 0$ the model is no longer integrable except in the non-interacting limit, $U = 0$, where H is diagonalized by Fourier transformation and has a single-electron spectrum

$$\varepsilon(k) = -2t \cos k + 2t' \cos 2k. \quad (2)$$

For $t' < 0.5t$, the electron band has two Fermi points at $k_F = \pm\pi/2$, separated from each other by the Umklapp vector $q = \pi$ (see Fig.2). In this case, a weak-coupling renormalization group analysis⁸ predicts the same behavior as for $t' = 0$ because the Umklapp term of order U is not modified; it again leads to the dynamical generation of a charge gap for $U > 0$, while the magnetic excitation spectrum remains gapless.

In the strong-coupling limit, $U \gg t, t'$, the charge sector is gapped, while the spin sector can be mapped onto

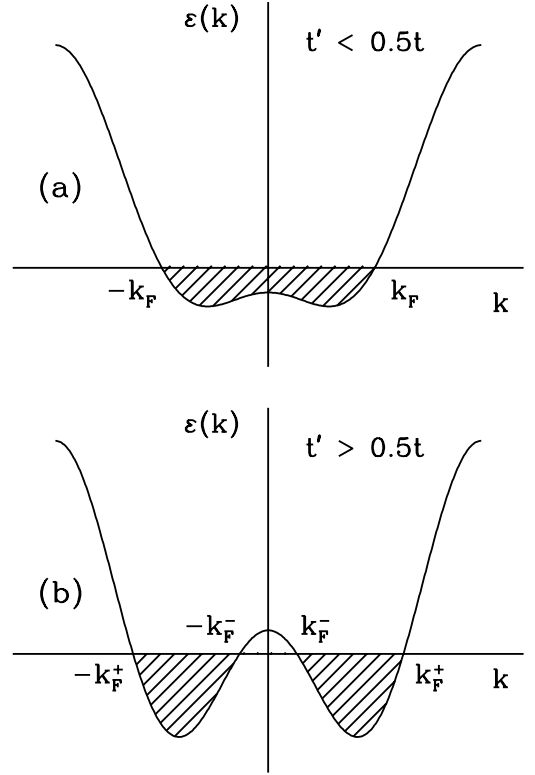


FIG. 2: Single-particle dispersion relation of the $t - t'$ chain for (a) $t' = 0.4t$ and (b) $t' = t$.

a frustrated Heisenberg chain

$$H = \sum_j (J \mathbf{S}_j \cdot \mathbf{S}_{j+1} + J' \mathbf{S}_j \cdot \mathbf{S}_{j+2}) \quad (3)$$

with $J = 4t^2/U$ and $J' = 4t'^2/U$. This model has been extensively studied using a number of different analytical methods^{21,22,23} and has been found to develop a spin gap for $J'/J \sim (t'/t)^2 > 0.2412$ ^{21,22} and incommensurate antiferromagnetic order for $J'/J > 0.5$.²³ This picture has been confirmed numerically.^{11,12}

For $t' > 0.5t$, the Fermi level intersects the one-electron band at four points ($\pm k_F^\pm$). This is the origin of more complex behavior for weak and intermediate values of U . For weak coupling ($U \ll t$), the ground-state phase diagram is well understood in the two-chain limit ($t' \gg t$).⁸ In this case, the Fermi vectors k_F^\pm are sufficiently far from $\pi/2$ to suppress first-order umklapp processes. Therefore, the system is metallic. The infrared behavior is governed by the low-energy excitations in the vicinity of the four Fermi points, in full analogy with the two-leg Hubbard model.²⁴ Thus, while the charge excitations are gapless, the spin degrees of freedom are gapped.^{8,12,13,15,24} Higher-order Umklapp processes become relevant for intermediate values of U because the Fermi momenta fulfill the condition $4(k_F^+ - k_F^-) = 2\pi$ (at half-filling). Therefore, starting from a metallic regime for small U at a

given value of t' ($t' > 0.5t$), one reaches a transition line $U = U_c(t')$, above which the system is insulating with both charge and spin gaps.⁸ The gross features of the phase diagram are depicted in Fig. 3.

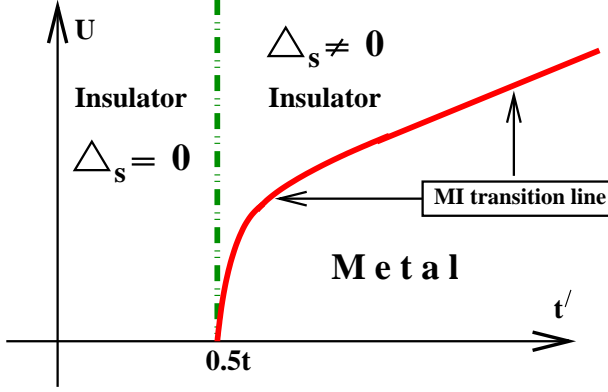


FIG. 3: Qualitative sketch of the ground state phase diagram of the half-filled $t - t'$ model. The solid line marks the metal-insulator transition. The dashed line indicates the transition from a gapless spin excitation spectrum at $t' \leq 0.5t$ to the spin-gapped phase.

III. BOSONIZATION

A. Effective Theory

We first consider the regime $U, t' \ll t$ where bosonization is applicable. We linearize the spectrum in the vicinity of the two Fermi points $k_F = \pm\pi/2$ and go to the continuum limit by substituting

$$c_{n\sigma} \rightarrow i^n \psi_{R\sigma}(x) + (-i)^n \psi_{L\sigma}(x), \quad (4)$$

where the operators $\psi_{R\sigma}(x)$ and $\psi_{L\sigma}(x)$ are the right and left components of the Fermi field, respectively. These fields can be bosonized in a standard way,²⁵

$$\begin{aligned} \psi_{R\sigma} &\rightarrow \frac{1}{\sqrt{2\pi\alpha}} e^{i\sqrt{4\pi}\phi_{R\sigma}} \\ \psi_{L\sigma} &\rightarrow \frac{1}{\sqrt{2\pi\alpha}} e^{-i\sqrt{4\pi}\phi_{L\sigma}}, \end{aligned}$$

where $\phi_{R\sigma}$ ($\phi_{L\sigma}$) are the right(left)-moving Bose fields and α is the infrared cutoff. We define $\phi_\sigma = \phi_{R\sigma} + \phi_{L\sigma}$ and introduce linear combinations, $\varphi_c = (\phi_\uparrow + \phi_\downarrow)\sqrt{2}$ and $\varphi_s = (\phi_\uparrow - \phi_\downarrow)\sqrt{2}$, to describe the charge and spin degrees of freedom, respectively. Correspondingly, we introduce the conjugate fields $\theta_\sigma = \phi_{L\sigma} - \phi_{R\sigma}$ and $\vartheta_c = (\theta_\uparrow + \theta_\downarrow)\sqrt{2}$ and $\vartheta_s = (\theta_\uparrow - \theta_\downarrow)\sqrt{2}$. After a simple rescaling, we arrive at the bosonized version of the Hamiltonian (1)

$$\mathcal{H} = \mathcal{H}_s + \mathcal{H}_c,$$

where both the spin part

$$\begin{aligned} \mathcal{H}_s = v_s \int dx &\left\{ \frac{1}{2}(\partial_x \varphi_s)^2 + \frac{1}{2}(\partial_x \vartheta_s)^2 \right. \\ &\left. + \frac{m_s^0}{2\pi\alpha^2} \cos(\sqrt{8\pi}\varphi_s) \right\}, \end{aligned} \quad (5)$$

and the charge part,

$$\begin{aligned} \mathcal{H}_c = v_c \int dx &\left\{ \frac{1}{2K_c}(\partial_x \varphi_c)^2 + \frac{K_c}{2}(\partial_x \vartheta_c)^2 \right. \\ &\left. + \frac{m_c^0}{2\pi\alpha^2} \cos(\sqrt{8\pi}\varphi_c) \right\}, \end{aligned} \quad (6)$$

are described by the massive sine-Gordon model, with parameters

$$\begin{aligned} v_s &\approx v_c \approx v_F, \\ (K_c - 1) &= -2m_s^0 = 2m_c^0 \approx -U/\pi t. \end{aligned} \quad (7)$$

There is an important difference between H_s and H_c due to the different stiffness constants. In the spin sector with $K_s = 1$, the system is in the weak-coupling limit and scales to a Gaussian model with gapless spin excitations. In the charge sector with $K_c < 1$, the system is in the strong coupling regime and the low-energy behavior is dominated by the cosine term. In the ground state, the field φ_c is pinned at one of the minima of the cosine term and, correspondingly, there is a finite energy gap for charge excitations.

Let us now discuss what happens when t' increases and reaches values of the order of $t/2$, where two additional Fermi points appear in the band structure. For spin degrees of freedom, new scattering channels appear at $t' = t/2$, and the system scales to strong coupling. Therefore, a spin gap is expected to open for $t' > t/2$, very much like in the case of two coupled Hubbard chains.²⁴

For the charge degrees of freedom, the situation is more complicated (and more interesting) because the charge gap blocks new scattering channels until t' is made sufficiently large so that additional states emerge beyond the gapped region. Thus, for t' slightly above $t/2$, the Fermi momentum changes without affecting the Umklapp processes. The Hamiltonian is still given by Eq. (6), but in order to allow for a change of particle number around the Fermi points, we have to add a topological (chemical potential) term

$$\delta H_c = -\frac{\mu_{\text{eff}}}{\sqrt{2\pi}} \int dx \partial_x \varphi_c, \quad (8)$$

where

$$\mu_{\text{eff}} = \begin{cases} 0 & \text{for } t' < 0.5t \\ \frac{t^2}{2t'} - 2t' \neq 0 & \text{for } t' > 0.5t. \end{cases} \quad (9)$$

$H_c + \delta H_c$ is the standard Hamiltonian for the commensurate-incommensurate transition,^{25,26} which has been intensively studied in the past using bosonization¹⁹ and the Bethe ansatz.²⁰

B. Commensurate-incommensurate transition

We now apply the theory of commensurate-incommensurate transitions to the metal-insulator transition as a function of t' . At $\mu_{\text{eff}} = 0$ and $K_c < 1$, the ground state of the field φ_c is pinned at

$$\langle 0 | \sqrt{8\pi} \varphi_c | 0 \rangle_0 = 2\pi n. \quad (10)$$

The presence of the effective chemical potential makes it necessary to consider the ground state of the sine-Gordon model in sectors with nonzero topological charge. Using the standard expression for charge density in the case of two Fermi points,²⁵

$$\begin{aligned} \rho_c(x) &\simeq \frac{1}{\sqrt{2\pi}} \partial_x \varphi_c \\ &+ A_{2k_F} \cos(2k_F x) \sin(\sqrt{2\pi} \varphi_c) \cos(\sqrt{2\pi} \varphi_s) \\ &+ A_{4k_F} \cos(4k_F x) \cos(\sqrt{8\pi} \varphi_c), \end{aligned} \quad (11)$$

we observe that the pinning of the field φ_c in one of the minima (10) suppresses the $2k_F$ charge fluctuations and stabilizes the $4k_F$ component. Any distortion of the $4k_F$ charge distribution would require an energy greater than the charge gap. This competition between the chemical potential term and commensurability drives a continuous phase transition from a gapped (insulating) phase at $\mu_{\text{eff}} < \mu_{\text{eff}}^c$ to a gapless (metallic) phase at

$$\mu_{\text{eff}} > \mu_{\text{eff}}^c = \Delta_c, \quad (12)$$

where Δ_c is the charge gap at $\mu_{\text{eff}} = 0$.

We now separately consider the qualitative behavior of the system in the following three parameter regimes: (i) $t' < 0.5t$, (ii) $0.5t < t' < t'_c$, and (iii) $t' > t'_c$, illustrated in Fig.4. In regime (i), $t' < 0.5t$, we expect a charge gap $\Delta_c(U, t') \approx \Delta_c(U, t' = 0)$ and no spin gap, as in the simple Hubbard model ($t' = 0$). In regime (ii), $0.5t < t' < t'_c$, the spin gap opens while the charge gap is reduced as²⁷

$$\Delta_c(U, t') = \Delta_c(U, 0.5t) - \mu_{\text{eff}}, \quad (13)$$

where μ_{eff} is given by Eq. (9). Therefore, the charge gap decreases with increasing t' and tends to zero at a t'_c qualitatively given by

$$\Delta_c(U, 0) - 2t'_c + t'^2/2t'_c = 0. \quad (14)$$

In regime (iii), $t' > t'_c$, the behavior of the system is characterized by four Fermi points, $\pm k_F^\pm$. The charge excitations are gapless, while the spin excitations are, generically, gapped.^{8,24} Charge fluctuations will be characterized by two dominant periodic modulations with wave vectors $2k_F^-$ and $2k_F^+$. For t' slightly larger than t'_c , the usual charge-density wave ($2k_F^+ \approx \pi$) is accompanied by a long-wavelength modulation at

$$2k_F^- = \sqrt{(t' - t'_c)/t'_c}. \quad (15)$$

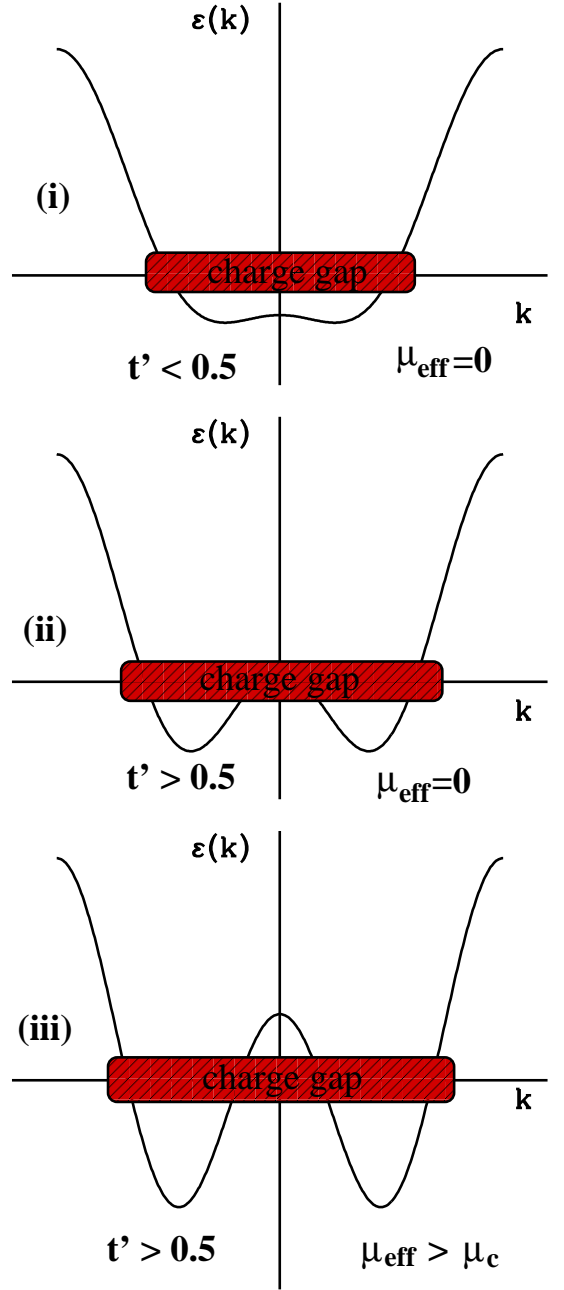


FIG. 4: Sketch of the energy dispersions for the three regimes (i), (ii), and (iii).

As soon as the new set of states in the vicinity of the Fermi points $\pm k_F^\pm$ appears, a channel for higher order umklapp scattering processes opens. In the sector of the phase diagram characterized by two-band behavior ($t' \gg t$), these processes are responsible for the opening of a charge gap at the transition line.⁸ Therefore, in the parameter range where the renormalized one-band (Hubbard) gap (13) becomes exponentially small, a crossover to the regime of two-band behavior takes place. Therefore, the linear decay of the charge gap as a function of

t' crosses over to exponential behavior. The evolution of the charge gap as a function of t' is sketched in Fig. 5.

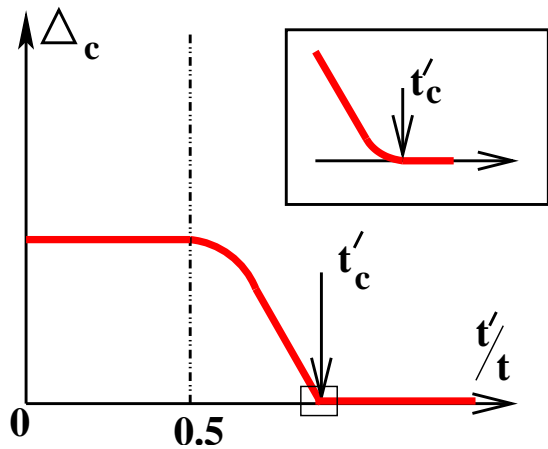


FIG. 5: Sketch of the charge gap as a function of the parameter t' . The inset shows an enlargement of the vicinity of the transition point.

C. Two-chain limit

To conclude our analysis, we discuss the limit of strong next-nearest-neighbor hopping ($t' \gg t$). For $t = 0$, the system is decoupled into two half-filled Hubbard chains and, for arbitrary $U > 0$, the ground state corresponds to a Mott insulator. The origin of the insulating behavior is the commensurability of umklapp scattering between the Fermi points, located at $\pm\pi/4$ and $\pm3\pi/4$. When $t \neq 0$ this commensurability is lost. The Fermi points are shifted with respect to their values at $t = 0$, and the Fermi energy (the chemical potential for $U = 0$) moves away from 0 to $\varepsilon_F \approx -t^2/2t'$ (for $t \ll t'$). For large enough values of t , the system is therefore expected to be metallic.

In order to estimate the location of the Mott transition, we can use a similar argument to the one given above for $t' \approx 0.5$. As long as the chemical potential is smaller than the charge gap, the system remains an insulator. A transition to a metallic phase is expected to occur for ε_F of the order of Δ_c , i.e., for $t^2 \approx (Ut'^3)^{1/2} \exp(-2\pi t'/U)$. A qualitative sketch of the phase diagram is given in Fig. 6.

IV. NUMERICAL RESULTS

In order to investigate the detailed behavior of the metal-insulator transition and to test the validity of the picture obtained from bosonization, we have carried out numerical calculations using the DMRG.²⁸ We have calculated the properties of the ground state and low-lying excited states for systems with open boundary conditions

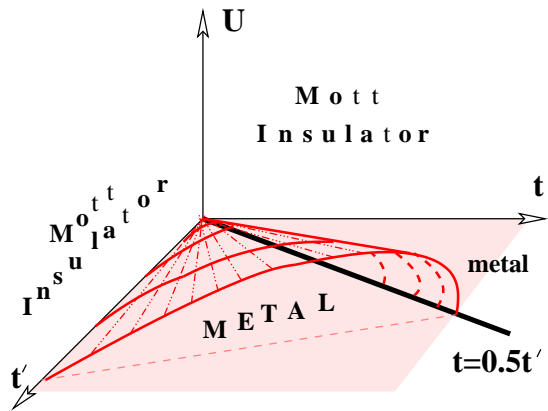


FIG. 6: Qualitative phase diagram of the half-filled repulsive $t - t'$ Hubbard chain. A gapless charge excitation spectrum (metallic phase) exists at $U = 0$ for arbitrary t and t' and for $U > 0$ in the sector of parameter space below the “roof” covering the area $U < U_c$ between the lines $t' = 0.5t$ and $t = 0$ in the $U = 0$ plane.

of lengths between $L = 32$ and $L = 128$ sites, keeping up to $m = 1000$ density-matrix eigenstates. As we shall see in the following, the finite-size effects are quite large in certain parameter regimes, so that a careful finite-size scaling must be carried out.

A. Transition line

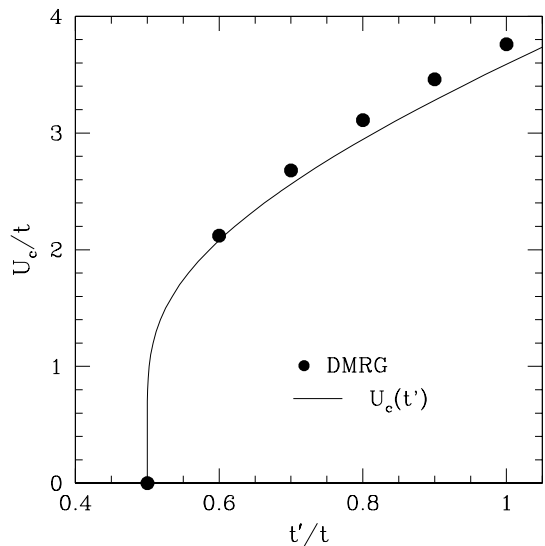


FIG. 7: The metal-insulator transition line in the $t - t' - U$ model with $t = 1$ obtained from DMRG studies^{14,29} (black circles) and from Eq. (14) (solid line).

The critical behavior of the metal-insulator transition as a function of U/t for $t' > 0.5t$ can be obtained from

the behavior of the electric susceptibility, which diverges in going from an insulator to a metal.^{14,29} In Fig. 7, we display the transition line in the $t-t'-U$ model at $t = 1$ obtained from the DMRG^{14,29} and from Eq. (14). The agreement between the DMRG results and Eq. (14) is remarkably good.

B. Spin and charge gaps

In order to investigate the predictions of the continuum theory, we calculate the charge gap, defined as

$$\Delta_c = \frac{1}{2} [E_0(N+2, 0) + E_0(N-2, 0) - 2E_0(N, 0)] \quad (16)$$

and the spin gap,

$$\Delta_s = E_0(N, 1) - E_0(N, 0), \quad (17)$$

where $E_0(N, S)$ is the ground-state energy for N particles and spin S on a chain of fixed length L , using the DMRG.

In Fig. 8, we display the spin gap as a function of t' at $U/t = 2$ and $U/t = 3$ for various values of the chain length L . As can be clearly seen, for $0 < t' \leq 0.5t$ the spin excitation spectrum on finite chains does not depend on t' . For $t' \leq 0.5t$, the value of the spin gap is found to coincide with that of the half-filled Hubbard model ($t' = 0$) which vanishes in the infinite-chain limit [see Fig. 9 (a)].

A clear change in the t' -dependence of the spin gap at $U/t = 2$ takes place at $t' = 0.5t$, indicating the development of a new phase in the spin sector. It is known from other studies^{8,12,13,15,24} that a spin gap opens at a critical value of t' which is approximately at or slightly above $t' = 0.5t$, becoming weakly larger at intermediate U values.

In Fig. 9(a), we display the spin gap plotted as a function of the inverse chain length for three values of t' near the transition at $U/t = 3$. At $t' = 0.55t$, the spin gap clearly scales to zero at infinite system size, with the values at a particular system size virtually identical to the $t' = 0$ case and the scaling predominantly linear in inverse system size. For $t' = 0.6t$ and $t' = 0.65t$, the dominant scaling term is quadratic rather than linear in $1/L$ and there is clearly scaling to a finite value of the gap. For $t' = 0.65t$, the size of the extrapolated gap is smaller than for $t' = 0.6t$, and there is a slight upturn in the gap at the largest system size, which, however, is not significantly larger than the estimated error of the DMRG calculation, approximately the symbol size. However, for larger values of t' , the finite-size behavior becomes less regular, as can be seen in Figs. 8(a) and (b). This behavior is due to the appearance of an incommensurate wave vector characterizing the spin excitations that occurs when a substantial density of states at all four Fermi points develops and makes it virtually impossible to carry out a well-controlled finite-size scaling for larger values of t' .

The transition associated with the opening of the spin gap is independent from the insulator-metal transition,

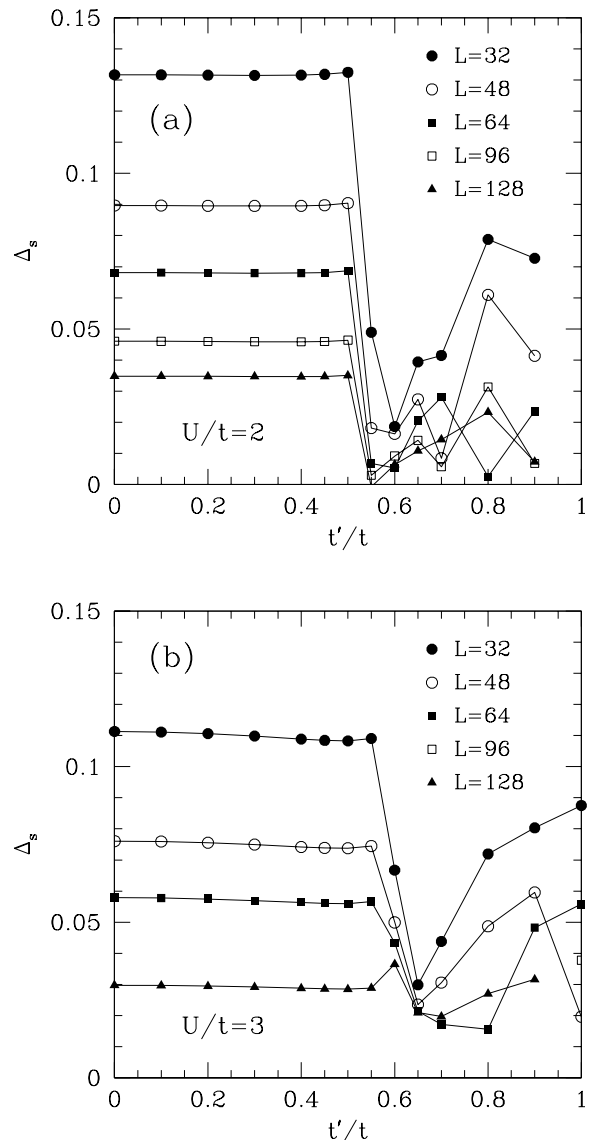


FIG. 8: Spin gap of as a function of t' for (a) $U/t = 2$ and (b) $U/t = 3$.

as can be clearly seen for $U/t = 3$ (where the effect of fluctuations is reduced). As is shown in Fig. 8(b) and Fig. 9(a), the spin gap opens for $t'_s \geq 0.55t$, while the insulator-metal transition takes place at $t'_c \simeq 0.65t$ (see below). Note that the critical value of the next-nearest-neighbor hopping amplitude, corresponding to an opening of the spin gap at $U/t = 3$, $t'_s \geq 0.55t$ deviates from the line $t'_s \geq 0.5t$. Our findings agree with previous studies.^{8,12,13,15,24}

A plot of the finite-size extrapolation of the charge gap is displayed in Fig. 9(b) for various values of t' . As can be seen, the behavior is well-behaved for values of t' from 0 to 0.8. For $0 \leq t' \leq 0.6t$, the scaling has a substantial positive quadratic term in $1/L$ and the gap is finite. For $t' = 0.65t$ and $0.8t$, the extrapolated gap clearly vanishes

and there is a negligible or negative quadratic contribution. For $t' > 0.8$, the finite-size effects become irregular due to incommensurability of the charge excitations, and finite-size extrapolation becomes difficult.

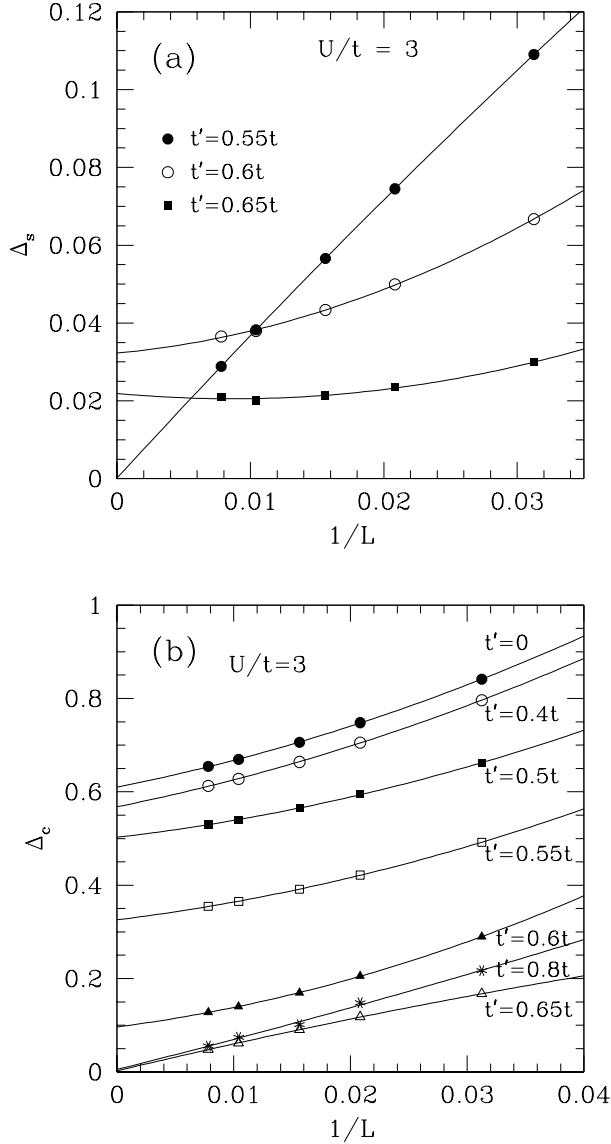


FIG. 9: (a) Spin gap and (b) charge gap as a function of $1/L$ for $U/t = 3$ and various values of t'/t .

In Fig. 10, the $L = \infty$ extrapolated value of the charge gap is displayed as a function of t' for $U/t = 2$ and $U/t = 3$. There is a clearly defined insulator-metal transition at $t_c = 0.55t$ at $U/t = 2$ and $t_c = 0.65t$ for $U/t = 3$. Note that the charge gap goes smoothly to zero above $t' = 0.5t$ for $U/t = 3$. The inset in Fig. 10 shows the charge gap for $U/t = 3$ as a function of the parameter $\mu_{\text{eff}} = 2t' - t^2/2t'$ for $0.5t < t' < 0.85t$. As can be seen, the charge gap drops off approximately linearly with μ_{eff} , in agreement with Eq. 13. For $U/t = 2$, there is a somewhat irregular behavior of the charge gap near the $t' = 0.5t$.

In particular, there is a small peak exactly at $t' = 0.5$. The finite-size scaling for this point is completely regular, however, and we estimate the size of the total error, due to both the extrapolation and the DMRG accuracy, to be less than the symbol size. Therefore, in our estimation, the peak at $t' = 0.5$ is a real effect. For $t' = 0.55$, the value of the extrapolated charge gap is slightly below zero. This is due to errors in the finite-size extrapolation due to slightly irregular behavior with system size.

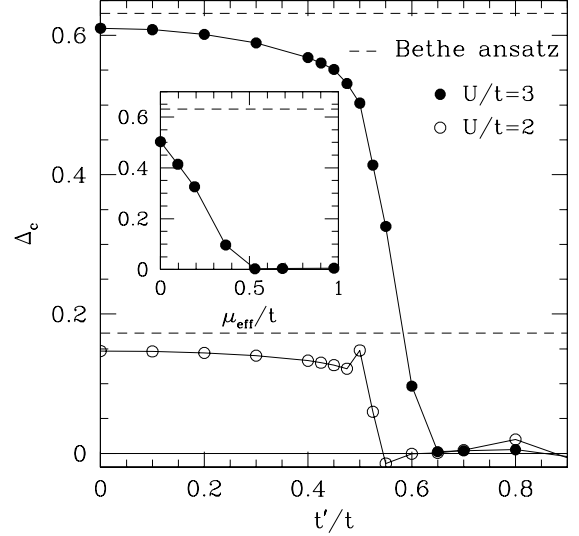


FIG. 10: Charge gap as a function of t' for $U/t = 3$ (black circles) and $U/t = 2$ (open circles). The inset shows the charge gap as a function of the parameter μ_{eff} for $0.5 < t' < 0.85t$.

C. Spin and charge densities

Valuable insight into the nature of the insulator-metal transition can be obtained by studying the charge and spin density distributions.

We first examine the local charge density $\langle n_i \rangle$ in the ground state with $L = 64$ sites and $U/t = 3$ as t' is varied. At $t' = 0.6t$, as can be seen in Fig. 11(a), the commensurate charge distribution characterizing the insulating phase (i.e., $\langle n_i \rangle = 1$) is reached within a few lattice sites from the edge. The boundary effect is relatively weak and short-range. The insulator-metal transition manifests itself at $t'_c = 0.65t$ via the appearance of incommensurate modulations in the charge distribution. One can clearly see the long-wavelength modulations in density originating from the opening of the Fermi surface for $|k| \leq K_F^-$. At $t' = 0.8t$, the incommensurability increases and the presence of long wavelength modulations of the charge density become more evident.

In Fig. 11(b), we plot the charge distribution at $t' = 0.8$ for various values U . In the metallic phase, at $U/t = 2$

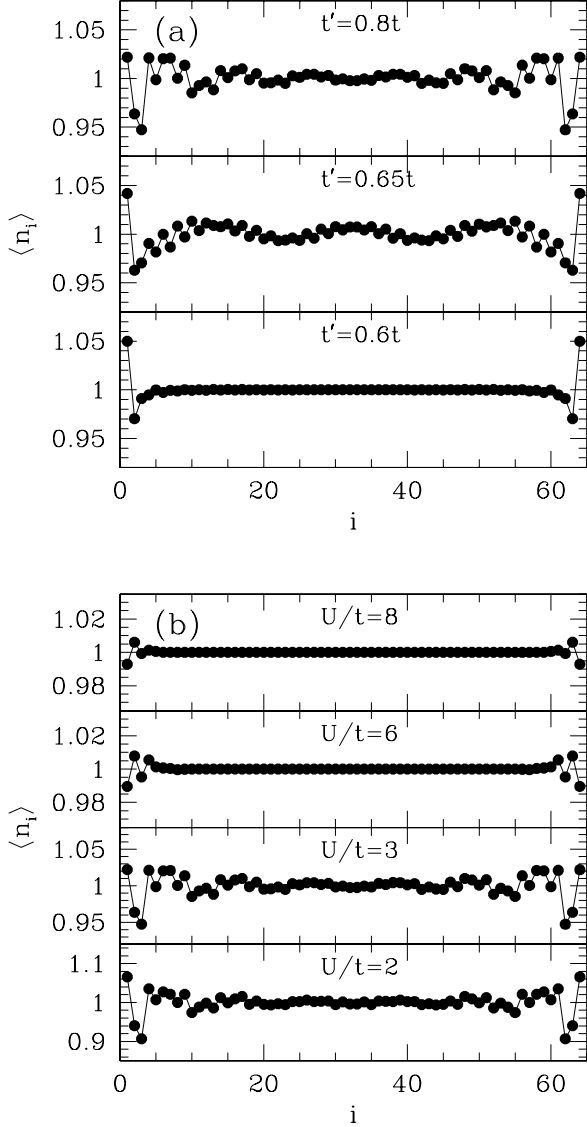


FIG. 11: Charge distribution $\langle n_i \rangle$ in the ground state of the $t - t' - U$ chain with (a) $L = 64$, $U/t = 3$ and $t' = 0.6t, 0.65t, 0.8t$ and (b) for $t' = 0.8t$ and $U/t = 2, 3, 6, 8$.

and $U/t = 3$, the charge distribution pattern is strongly incommensurate. At $U/t = 6$ and $U/t = 8$, the well-established commensurate pattern of the charge distribution characterizes the insulating phase.

Let us now consider the spin density distribution. As has already been stressed above, due to spin-charge separation, the magnetic degrees of freedom in the $t - t' - U$ Hubbard model are not influenced by the destruction of the “holon Fermi surface” caused by the dynamical generation of a charge gap. Instead, the development of the incommensurate spin distribution in the insulating phase is completely determined by the competition between the nearest-neighbor and next-nearest-neighbor spin exchange interactions and reflects the itinerant na-

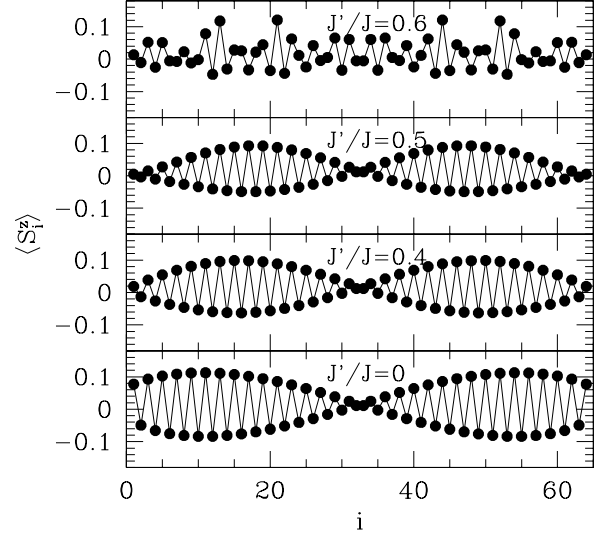


FIG. 12: Spin distribution $\langle S_i^z \rangle$ in the $S_{\text{total}}^z = 1$ state of the frustrated Heisenberg chain with $L = 64$ and $J'/J = 0, 0.4, 0.5$, and 0.6 .

ture of the model only when the system is very close to the insulator-metal transition or is in the metallic phase. To see this, we examine the behavior of the spin distribution $\langle S_i^z \rangle$ in the $S_{\text{total}}^z = 1$ excited state of the $t - t' - U$ Hubbard model, comparing it to the effective model for strong coupling, the frustrated Heisenberg chain.

We first examine the limiting case of the frustrated Heisenberg chain, Hamiltonian (3). In Fig. 12, we plot $\langle S_i^z \rangle$ calculated using the DMRG in the $S_{\text{total}}^z = 1$ state for various values of the next-nearest-neighbor exchange J' . At $J' = 0$, the unfrustrated case, there is one node in the distribution of the spin density, which corresponds to two spatially separated spin- $S = 1/2$ spinons.³⁰ These two spinons characterize the spin excitations up to the Majumdar-Ghosh point $J' = 0.5J$ ($t' \simeq 0.7t$).³¹ For larger values of the next-nearest-neighbor exchange, the spin distribution becomes incommensurate.²³ In the plot for $J'/J = 0.6$, the absence of the commensurate two-spinon structure of the excitations and the appearance of the incommensurate wave vector can be seen.

We next examine the behavior for the $t - t' - U$ chain. In Fig 13, we show the spin distribution $\langle S_i^z \rangle$ in the $S_{\text{total}}^z = 1$ state with $L = 64$, $U/t = 3$ and various values of t' . The single-node pattern characteristic of two spinons, as found in the unfrustrated and weakly frustrated Heisenberg chain, can be seen for $t' = 0.6t$ and smaller. At $t' = 0.7t$ an incommensurate pattern appears. This is just above the value of t' at which the charge gap goes to zero, $t'_c \simeq 0.65t$, (see Fig. 10) and the system becomes metallic. However, for $t' > 0.7t$ the point at which the spin-density distribution becomes incommensurate is independent of the insulator-to-metal transition. To demonstrate this, we plot the spin density

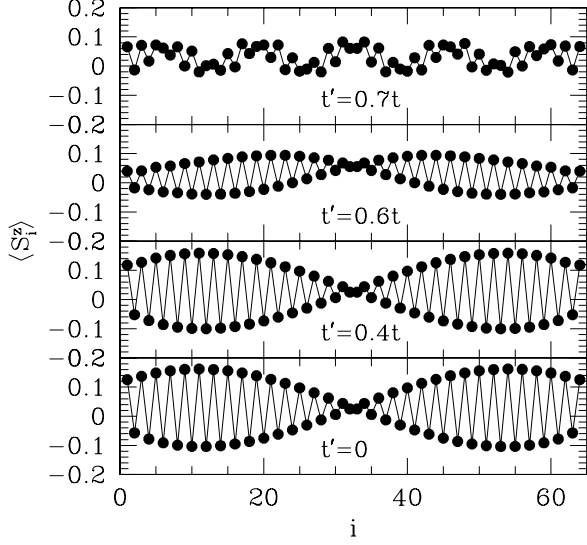


FIG. 13: Spin distribution $\langle S_i^z \rangle$ in the $S_{\text{total}}^z = 1$ state of the $t - t' - U$ chain with $L = 64$, $U/t = 3$ and $t' = 0, 0.4t, 0.6t$, and $0.7t$.

distribution in the $S_{\text{total}}^z = 1$ state for increasing on-site repulsion U for $t' = 0.6t$ and $t' = 0.8t$ in Fig. 14. As can be seen in Fig. 14(a), for $t' = 0.6t$ the spin-density distribution is incommensurate in the metallic phase at $U/t = 2$, but acquires the commensurate single-node pattern characteristic of two spinons for on-site repulsions of $U/t = 3$ and higher. In contrast, for $t' = 0.8t$, Fig. 14(b), the incommensurate pattern of the spin distribution in the metallic phase ($U/t = 2$) remains not only in the vicinity of the insulator-metal transition at $U/t = 3$ but also deep into the insulating phase at $U/t = 8$ and $U/t = 10$.

D. Excitations for Large t'

We examine the behavior of the $t - t' - U$ chain for large next-nearest hopping ($t' \gg t$), a limit which corresponds to two chains coupled with a weak zigzag hopping. In particular, we numerically investigate the transition from a two-chain (four-Fermi-point) metallic regime at weak U to the strong-coupling regime, for which the effective model is two spin- $S = 1/2$ Heisenberg chains coupled with a frustrating zigzag interaction at $U \gg t' \gg t$, i.e., $J' \gg J$.

In Fig. 15, we show the charge distribution $\langle n_i \rangle$ in the ground state of the $t - t' - U$ chain for $t' = 3t$, $L = 64$, and $U/t = 4, 8, 10$, and 20. In the metallic phase ($U/t = 4$ and $U/t = 8$), the relative charge density on the two chains alternates with relatively strong amplitude and is modulated by an incommensurate wave vector. As U/t is increased to 10, the amplitude of the charge fluctuations between the chains is strongly suppressed and

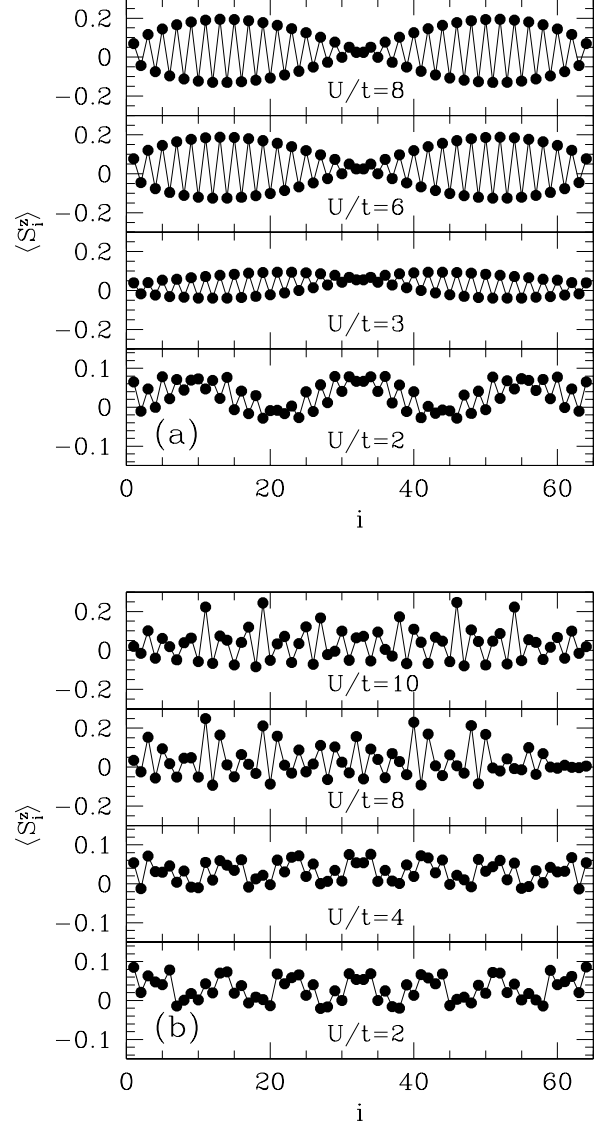


FIG. 14: Spin distribution $\langle S_i^z \rangle$ in the $S_{\text{total}}^z = 1$ state of the $t - t' - U$ chain with $L = 64$ and for (a) $t' = 0.6t$ with $U/t = 2, 3, 6, 8$ and (b) $t' = 0.8t$ with $U/t = 2, 4, 8, 10$.

the incommensurate structure of the charge distribution changes to a very distinctive two-bubble pattern. This two-bubble distribution corresponds to two spatially separated electron-hole pairs with an electron on even chain and a hole on odd chain in the left part of the lattice and the inverse configuration in the right half of the lattice. (Note that the ends break the symmetry between the two chains.) Deeper into the insulating phase, at $U/t = 20$, the charge density is almost smooth and equal between the chains, except for a small residual alternation of charge density due to the end effects.

In Fig. 16, we show the spin density distribution $\langle S_i^z \rangle$ in the $S_{\text{total}}^z = 1$ state for $t' = 3t$ and $U/t = 4, 8, 10, 20$. As can be seen, the incommensurate pattern of the

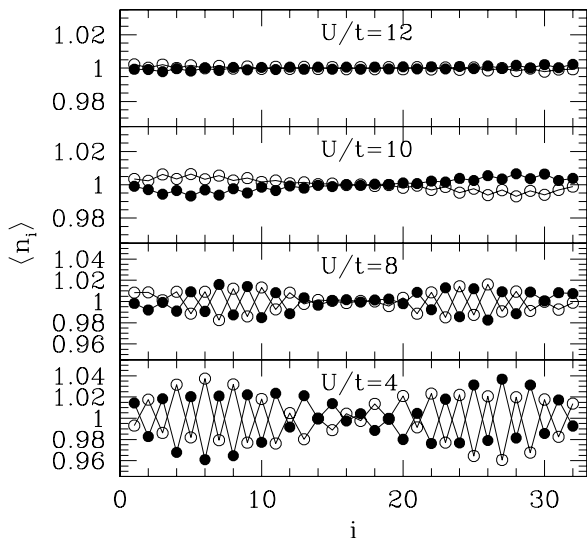


FIG. 15: Charge distribution $\langle n_i \rangle$ in the ground state of the $t - t' - U$ chain with $L = 64$, $t' = 3t$ and $U/t = 4, 8, 10, 20$. Black circles correspond to odd and open circles to even lattice sites.

spin distribution in the metallic phase at $U/t = 4$ and $U/t = 5$ transforms in the insulating phase ($U/t = 10$ and $U/t = 12$) into a pattern which, for each chain, is similar to that of the single Heisenberg chain in the commensurate phase. This pattern, seen in, e.g., Fig. 12 for $J'/J = 0, 0.4, 0.5$, corresponds to two-spinon excitations, as previously discussed. This indicates that the system behaves as two identical, weakly coupled $S = 1/2$ Heisenberg chains at large U .

V. CONCLUSIONS

We have carried out a combined analytical and numerical analysis of the insulator-metal transition in the half-filled one-dimensional $t - t' - U$ model. Using the weak-coupling bosonization approach, we have shown that the gross features of the transition from an insulator to metal as a function of next-nearest-neighbor hopping t' can be described within the standard theory of commensurate-incommensurate transitions. We have derived an explicit expression for the critical line $t'_c(U)$ separating the metallic phase from the spin-gapped insulator. We have also argued that in the vicinity of transition line a crossover to infinite-order critical behavior occurs.

Using DMRG calculations on chains of up to $L = 128$ sites, we have performed a detailed numerical analysis of the excitation spectrum and the charge and spin density distributions in various sectors of the phase diagram. In particular, we have studied the evolution of the charge

and spin gap with increasing next-nearest-neighbor hopping amplitude t' . We have found evidence for a spin

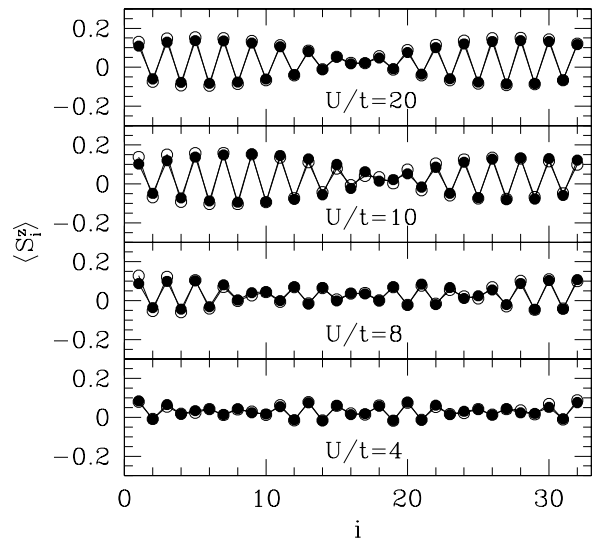


FIG. 16: Spin distribution $\langle S_i^z \rangle$ in the $S_{\text{total}}^z = 1$ state of the $t - t' - U$ chain with $L = 64$, $t' = 3t$ and $U/t = 4, 8, 10, 20$. Black circles correspond to lattice odd and open circles to even lattice sites.

gap in the parameter range $0.5t < t' < t'_c$, in agreement with previous studies. We have shown that the change in the topology of Fermi surface at the insulator-metal transition is reflected in the appearance of incommensurate modulations of the charge density. Incommensurate spin-density distributions in the triplet sector are always present in the metallic phase, but can also appear independently in the spin-gapped insulator due to frustration.

For $t' \gg t$, we have argued that the insulator-metal transition can be best understood starting from the limit of two uncoupled chains. At small U , turning on the zigzag coupling between the chains destroys the commensurability present for a single chain, and leads to a metallic phase. At large U , the system is insulating and behaves as two weakly coupled Heisenberg chains. We have estimated that the insulator-metal transition in this regime occurs when the shift in the Fermi energy is comparable to the size of the charge gap in the isolated Hubbard chain.

Acknowledgments

It is a pleasure to thank A. Aligia, C. Gros, A. Kampf, B. Normand, D. Poilblanc, and M. Sekania for interesting discussions. DB and GIJ also acknowledge support through the SCOPES grant 7GEPJ62379.

-
- * Permanent address: Andronikashvili Institute of Physics, Georgian Academy of Sciences, Tamarashvili 6, 0177 Tbilisi, Georgia
- ¹ N. F. Mott, *Metal-Insulator Transitions*, 2nd ed., Taylor and Francis, London (1990).
 - ² F. Gebhard, *The Mott Metal-Insulator Transition*, Springer, Berlin (1997).
 - ³ M. Imada, A. Fujimori, and Y. Tokura, *Rev. Mod. Phys.* **70**, 1039 (1998).
 - ⁴ M. Dzierzawa, D. Baeriswyl and L. M. Martelo, *Helv. Phys. Acta* **70**, 124 (1997).
 - ⁵ E. H. Lieb and F. Y. Wu, *Phys. Rev. Lett.* **20**, 1445 (1968).
 - ⁶ A. A. Ovchinnikov, *Sov. Phys. JETP* **30**, 1160 (1970).
 - ⁷ For a recent review see F. H. L. Essler, H. Frahm, F. Göhmann, A. Klümper, and V. E. Korepin, *The One-Dimensional Hubbard Model*, Cambridge Univ. Press, Cambridge (2005).
 - ⁸ M. Fabrizio, *Phys. Rev. B* **54**, 10054 (1996).
 - ⁹ K. Kuroki, R. Arita, and H. Aoki, *J. Phys. Soc. Japan* **66**, 3371 (1997).
 - ¹⁰ S. Daul and R. M. Noack, *Phys. Rev. B* **58**, 2635 (1998).
 - ¹¹ R. Arita, K. Kuroki, H. Aoki, and M. Fabrizio, *Phys. Rev. B* **57**, 10324 (1998).
 - ¹² S. Daul and R. M. Noack, *Phys. Rev. B* **61**, 1646 (2000).
 - ¹³ M. E. Torio, A. A. Aligia, and H. A. Ceccatto, *Phys. Rev. B* **67**, 165102 (2003).
 - ¹⁴ C. Aebischer, D. Baeriswyl, and R. M. Noack, *Phys. Rev. Lett.* **86**, 468 (2001).
 - ¹⁵ K. Louis, J. V. Alvarez, and C. Gros, *Phys. Rev. B* **64**, 113106 (2001); **65**, 249903(E) (2002).
 - ¹⁶ K. Hamacher, C. Gros, and W. Wenzel, *Phys. Rev. Lett.* **88**, 217203 (2002).
 - ¹⁷ C. Gros, K. Hamacher, and W. Wenzel, *Europhys. Lett.* **69**, 616 (2005).
 - ¹⁸ M. Capello, F. Becca, M. Fabrizio, S. Sorella, and E. Tosatti, *Phys. Rev. Lett.* **94**, 026406 (2005).
 - ¹⁹ G. I. Japaridze and A. A. Nersesyan, *JETP Pis'ma* **27**, 356 (1978); [*JETP Lett.* **27**, 334 (1978)]; *J. Low Temp. Phys.* **37**, 95 (1979); V. L. Pokrovsky and A. L. Talapov, *Phys. Rev. Lett.* **42**, 65 (1979); H. J. Schulz, *Phys. Rev. B* **22**, 5274 (1980).
 - ²⁰ G. I. Japaridze, A. A. Nersesyan, and P. B. Wiegmann, *Nucl. Phys. B* **230**, 511 (1984).
 - ²¹ F. D. M. Haldane, *Phys. Rev. B* **25**, 4925 (1982); **26**, 5257(E) (1982).
 - ²² K. Okamoto and K. Nomura, *Phys. Lett. A* **169**, 422 (1992); S. Eggert, *Phys. Rev. B* **54**, R9612 (1996).
 - ²³ S. R. White and I. Affleck, *Phys. Rev. B* **54**, 9862 (1996).
 - ²⁴ L. Balents and M. P. A. Fisher, *Phys. Rev. B* **53**, 12133 (1996).
 - ²⁵ A. O. Gogolin, A. A. Nersesyan, and A. M. Tsvelik, *Bosonization and Strongly Correlated Systems*, Cambridge Univ. Press, Cambridge (1998).
 - ²⁶ T. Giamarchi, *Quantum Physics in One Dimension*, Clarendon Press, Oxford (2004).
 - ²⁷ For details we refer to Chapter 17 in Ref. 25.
 - ²⁸ S. R. White, *Phys. Rev. Lett.* **69**, 2863 (1992); *Phys. Rev. B* **48**, 10345 (1993).
 - ²⁹ C. Aebischer, Ph. D. thesis, University of Fribourg, 2002, available at <http://ethesis.unifr.ch/theses>.
 - ³⁰ E. Sorensen, I. Affleck, D. Augier, and D. Poilblanc, *Phys. Rev. B* **58**, R14701 (1998).
 - ³¹ C. K. Majumdar and D. K. Ghosh, *J. Math. Phys.* **10**, 1388 (1969).